1   **Mathematical Analysis of Robustness of Oscillations in Models**

2   **of the Mammalian Circadian Clock**

3   **Short title: Robustness of Oscillations in Models of the Mammalian Circadian Clock**

4

5   Benjamin Heidebrecht[1], Jing Chen[1,2,3,*], & John J. Tyson[1,2,3,*]

6

7   [1]Division of Systems Biology, Virginia Tech, Blacksburg, VA 24061.

8   [2]Department of Biological Sciences, Virginia Tech, Blacksburg, VA, 24061

9   [3]Fralin Life Sciences Institute, Virginia Tech, Blacksburg, VA, 24061

10   * Co-corresponding authors. Email: chenjing@vt.edu, tyson@vt.edu

11

13

15

16   **ABSTRACT**

17   A wide variety of organisms possess endogenous circadian rhythms (~24 h period), which

18   coordinate many physiological functions with the day-night cycle. These rhythms are mediated

19   by a molecular mechanism based on transcription-translation feedback. A number of

20   mathematical models have been developed to study features of the circadian clock in a variety

21   of organisms. In this paper, we use bifurcation theory to explore properties of mathematical

22   models based on Kim & Forger's interpretation of the circadian clock in mammals. Their models

23   are based on a simple negative feedback (SNF) loop between a regulatory protein (PER) and its

24   transcriptional activator (BMAL). In their model, PER binds to BMAL to form a stoichiometric

25   complex (PER:BMAL) that is inactive as a transcription factor. However, for oscillations to occur

26   in the SNF model, the dissociation constant of the PER:BMAL complex, K_d, must be smaller than

27   10^{-3} nM, orders of magnitude below the limit set by the biophysics of protein binding. We have

28   relaxed this constraint by introducing two modifications to Kim & Forger's SNF model: (1)

29   replacing the first-order rate law for degradation of PER in the nucleus by a Michaelis-Menten

30   rate law, and (2) introducing a multistep reaction chain for posttranslational modifications of PER.

31   These modifications significantly increase the robustness of oscillations, and increase the

32   maximum allowable K_d to more reasonable values, 1—100 nM. In a third modification, we

33   considered alternative rate laws for gene transcription to resolve an unrealistically large rate of

34   *PER* transcription at very low levels of BMAL transcription factor. Additionally, we studied Kim &

35   Forger's extensions of the SNF model to include a second negative feedback loop (involving REV-

36   ERB) and a supplementary positive feedback loop (involving ROR). We found that the

2

37   supplementary positive feedback loop—but not the supplementary negative feedback loop—

38   provides additional robustness to the clock model.

39

40

41   **AUTHOR SUMMARY**

42   The circadian rhythm aligns bodily functions to the day/night cycle and is important for our

43   health. The rhythm originates from an intracellular, molecular clock mechanism that mediates

44   rhythmic gene expression. It is long understood that transcriptional negative feedback with

45   sufficient time delay is key to generating circadian oscillations. However, some of the most

46   widely cited mathematical models for the circadian clock suffer from problems of parameter

47   "fragilities". That is, sustained oscillations are possible only for physically unrealistic parameter

48   values. A recent model by Kim and Forger nicely incorporates the inhibitory binding of PER, a

49   key clock protein, to its transcription activator BMAL, but oscillations in their model require a

50   binding affinity between PER and BMAL that is orders of magnitude lower than the physical

51   limit of protein-protein binding. To rectify this problem, we make several physiologically

52   credible modifications to the Kim-Forger model, which allow oscillations to occur with realistic

53   binding affinity. The modified model is further extended to explore the potential roles of

54   supplementary feedback loops in the mammalian clock mechanism. Ultimately, accurate

55   models of the circadian clock will provide predictive tools for chronotherapy and chrono-

56   pharmacology studies.

3

57 **INTRODUCTION**

58 Most organisms experience perpetual day/night cycles and need to synchronize their

59 physiological functions with this potent external driving rhythm of light and temperature (1).

60 Endogenous circadian rhythms meet this demand. Across animals, plants, fungi and

61 cyanobacteria, nearly all circadian rhythms share four major physiological characteristics (2).

62 First, circadian rhythms are autonomous, meaning their timekeeping persists in the absence of

63 external light/dark cues. Second, circadian rhythms are temperature-compensated, meaning that

64 the autonomous cycle's period is quite resistant to temperature variations over a physiological

65 range (3-5). Third, circadian rhythms can be entrained to light/dark cycles considerably different

66 from 24 hours (6); e.g., mammals can entrain to light/dark periods from 20.5 to 27.5 h (7). Fourth,

67 the autonomous circadian rhythm can be phase-shifted by brief light exposures or temperature

68 pulses. These perturbations cause a permanent shift in the phase of the oscillation without

69 changing its period. This property underlies the familiar discomfort of 'jet lag' experienced by

70 transcontinental travelers (8).

71 The circadian rhythms are generated by molecular clock mechanisms that generate oscillations

72 of ~24h period through transcriptional-translational feedback (1, 9, 10). Although the genes and

73 proteins constituting the circadian clocks in animals, plants and fungi are quite different, their

74 essential interactions are remarkably similar. In all cases, the clock mechanism features a 'core'

75 negative feedback loop: *A activates B activates C inhibits A*. In mammals, this loop consists of

76 transcriptional regulation involving six genes: *PER1/2*, *CRY1/2*, *BMAL1*, and *CLOCK* (1, 9-11). For

77 convenience, in this work we drop the distinction between the homologous pairs of proteins

78 PER1/2 and CRY1/2. In this mechanism (Figure 1), the heterodimeric transcription factor

4

79   BMAL:CLOCK activates *PER* transcription. *PER* mRNA is then translated in the cytoplasm, where

80   PER protein binds with CRY and enters the nucleus. PER:CRY then binds with BMAL:CLOCK to

81   block its activation of *PER* transcription. PER:CRY's cycle of production, nuclear entry, auto-

82   inhibition, and subsequent degradation is widely acknowledged to be the source of circadian

83   rhythmicity (12). BMAL:CLOCK contributes to genome-wide rhythmic transcription; for instance,

84   in mouse liver, BMAL:CLOCK targets the enhancers of ~1,300 genes, out of which ~26% are

85   rhythmically transcribed (13). Additional transcriptional regulation comes from REV-ERB and ROR

86   proteins. BMAL:CLOCK activates the expression of their genes, and subsequently, cytoplasmic

87   ROR and REV-ERB proteins are translocated into the nucleus where they compete for repression

88   (by REV-ERB) or activation (by ROR) of *BMAL1* transcription (Figure 1) (1, 9-11). Ultimately,

89   3—15% of genes are rhythmically expressed in any tissue at any time (14), and the clock

90   transcription factors play important roles in this program (13, 15).

91   Over the past 50 years, many people have proposed mathematical models of circadian rhythms

92   (3, 12, 16-20). In 1965, Brian Goodwin proposed a model of periodic enzyme synthesis based on

93   negative feedback on gene expression (21, 22). Goodwin was not attending to circadian rhythms,

94   at the time, because nothing was known then about the negative feedback of PER on its own

95   synthesis. But his model was picked up later by Peter Ruoff (5, 23-25) to explain the characteristic

96   features of circadian rhythms. Recently, the core negative feedback loop of Goodwin's model

97   was extended with other feedback loops (as in Figure 1) to create more comprehensive and

98   realistic models of circadian rhythms (26-28). One particularly interesting modification to

99   Goodwin's model was made by Jae Kyoung Kim and Daniel Forger (27), who replaced Goodwin's

100   view of negative feedback by cooperative multimeric binding of a generic 'repressor' to a gene

5

101   promoter with their own model of stoichiometric binding of PER:CRY (a repressor) to

102   BMAL:CLOCK (an activator) of gene expression. Some characteristic features of the two models

103   were compared in (29). While all of these models have much to commend, they suffer from some

104   technical problems (parameter 'fragilities') that limit their appeal. In the following section, we

105   outline these difficulties, in order to frame our proposals for more robust and realistic

106   mathematical models of circadian clocks. Then, in the 'Results and Discussion' section, we

107   present our results in detail.

108   **PRELIMINARY MODELING ISSUES**

109   **Goodwin's Model**

110   To account for observations of periodic enzyme synthesis in bacteria (30), Brian Goodwin (21, 22)

111   presented the following model for the periodic synthesis of a protein Y from its mRNA X, where

112   mRNA synthesis is inhibited by a repressor Z:

$$\frac{dX}{dT} = \alpha_1 \frac{K^p}{K^p + Z^p} - \beta_1 X \qquad\qquad \frac{dx}{dt} = \alpha \frac{1}{1 + z^p} - x \qquad (1)$$

$$\frac{dY}{dT} = \alpha_2 X - \beta_2 Y \qquad\qquad \frac{dy}{dt} = x - y \qquad (2)$$

$$\frac{dZ}{dT} = \alpha_3 Y - \beta_3 Z \qquad\qquad \frac{dz}{dt} = y - z \qquad (3)$$

113

114   In Eq. (1), the factor $\frac{K^p}{K^p + Z^p}$ is the probability that the promoter region of the gene encoding X is

115   <u>not</u> bound to Z, its inhibitor, and α_1 is the maximum rate of synthesis of X by the gene. The other

116   terms in these equations correspond to first-order rate laws for production and removal of X, Y

117   and Z. In this tableau, Goodwin's equations are written in two equivalent forms. On the left, the

118   equations are written in terms of the original dimensional variables: concentrations X, Y and Z

119   (nM) and time T(h); on the right, in terms of the 'dimensionless' variables $x = \frac{\alpha_2 \alpha_3}{\beta_1^2} \cdot \frac{X}{K}$, $y = \frac{\alpha_3}{\beta_1} \cdot$

120    $\frac{Y}{K}$, $z = \frac{Z}{K}$, dimensionless time $t = \beta_1 T$, and a dimensionless parameter $\alpha = \frac{\alpha_1 \alpha_2 \alpha_3}{K \beta_1^3}$. In deriving

121   these dimensionless equations, we have assumed (as have all authors in the past) that $\beta_1 = \beta_2 =$

122   β_3, which serves to maximize the oscillatory potential of the model (31, 32). In Goodwin's version

123   of a three-component negative-feedback loop, the repression of gene transcription by Z is

124   modeled by a Hill function with exponent p. Underlying this function is the supposition that the

125   gene encoding X is turned off when p molecules of Z bind cooperatively to its promoter region

126   (or, equivalently, when p molecules of Z bind cooperatively to an activator of gene transcription

127   and shut it off).

128   <u>A problem with Goodwin's model</u>. J.S. Griffith (33) was first to point out that Goodwin's equations

129   (1)-(3) admit oscillatory solutions only if $p > \sec^3(\pi/3) = 8$, a very restrictive condition,

130   because in experimental studies it is rare that more than 3 or 4 proteins bind cooperatively to

131   DNA regulatory sequences (34). This condition becomes even more restrictive if $\beta_1 \neq \beta_2 \neq \beta_3$

132   (31).

133   <u>One solution: a longer feedback loop</u>. The restriction $p > 8$ can be ameliorated by lengthening the

134   feedback loop: if n = number of variables in the feedback loop, then the condition becomes $p >$

135    $\sec^n(\pi/n)$. For example, for $n = 8$, the condition is $p > 1.88$. Longer loops ($n > 3$) correspond to

136   inserting more than one intermediate (say, Y_0, Y_1, …, Y_{n-3}) between X (mRNA) and Z (feedback

137   component). This is quite reasonable, considering that PER protein has multiple phosphorylation

138   sites (35). Each intermediate, Y_j, then denotes cytoplasmic PER phosphorylated on j sites, $j = 0$,

7

139 1, …, $n-3$. Eventually, the fully phosphorylated form, Y_{n-3}, is transported into the nucleus and

140 becomes Z. In this case, Goodwin's dimensionless differential equations become Eqs. (4)-(7).

$$\frac{dx}{dt} = \alpha \frac{1}{1 + z^p} - x \tag{4}$$

$$\frac{dy_0}{dt} = x - y_0 \tag{5}$$

$$\frac{dy_m}{dt} = y_{m-1} - y_m, \qquad \text{for } m = 1, \dots, n-3 \tag{6}$$

$$\frac{dz}{dt} = y_{n-3} - z \tag{7}$$

141

142 Exactly the same equations can be derived by assuming a distributed time lag between X and Z

143 (36) and introducing the new variables

$$y_m(t) = \int_{-\infty}^{t} G_m(t - s) y_0(s) ds, \qquad \text{for } m = 1, \dots, n-2 \tag{8}$$

144

145 where $y_0(t)$ is the dimensionless form of $Y_0(T)$, and $G_m(u) = u^{m-1} e^{-u}/(m-1)!$ for integer

146 values of m. From this definition we can show that

$$\frac{dy_m}{dt} = y_{m-1} - y_m, \qquad \text{for } m = 1, \dots, n-3 \tag{9}$$

147

148 which is exactly Eq. (6) above.

8

149   A second solution: Michaelis-Menten degradation of Z. In 1982 Bliss, Painter and Marr (37)

150   proposed to replace the first-order degradation of Z, $-\beta_3 Z$, by a Michaelis-Menten rate law,

151    $-\beta_3 Z/(K_m + Z)$, where K_m is the 'Michaelis' constant of the enzyme-catalyzed reaction and β_3

152   is the 'V_{max}' of the reaction. With this change, the Goodwin model can exhibit limit cycle

153   oscillations even for $p = 1$ (37). The substitution of Michaelis-Menten rate laws for the first-order

154   kinetic terms in Eqs. (1)-(3) has been exploited by many authors (17, 38, 39) to increase the

155   robustness of their models of circadian rhythms.

156   **Kim & Forger's Model**

157   In 2012, Kim and Forger (27) presented a slightly different model of the negative feedback loop

158   controlling mammalian circadian rhythms (Figure 2a). In dimensionless form, the Kim-Forger (KF)

159   ODEs are:

160   Kim-Forger SNF Model.

$$\frac{dM}{dt} = \varphi \frac{A_{\text{free}}}{A_T} - M \tag{10}$$

$$\frac{dP_c}{dt} = M - P_c \tag{11}$$

$$\frac{dP}{dt} = P_c - P \tag{12}$$

$$A_{\text{free}} = \frac{1}{2}\left[A_T - P - K_d + \sqrt{(A_T - P - K_d)^2 + 4K_d A_T}\right] \tag{13}$$

161

9

162   SNF stands for 'simple negative feedback loop' (i.e., the negative feedback loop involving PER:CRY

163   inhibition of BMAL:CLOCK). As originally written, the KF model has three dynamical variables: M

164   = [*PER* mRNA], P_c = [PER protein in the cytoplasm], P = [PER protein in the nucleus] (i.e., PER:CRY

165   in the nucleus). The BMAL:CLOCK transcription factor is denoted by A; A_T is the total

166   concentration of BMAL:CLOCK in the nucleus, and A_{free} is the concentration of 'free' BMAL:CLOCK

167   in the nucleus. The factor A_{free}/A_T is the probability that BMAL:CLOCK is <u>not</u> bound to its

168   repressor, PER:CRY. By expressing the rate of transcription of *PER* mRNA to be proportional to

169   A_{free}/A_T, Kim & Forger are implicitly assuming that the total number of BMAL:CLOCK dimers is

170   large enough to saturate the E-boxes on the *PER* genes, and that PER:CRY binds equally well to

171   BMAL:CLOCK dimers that are either bound or not bound to an E-box (Supplementary Materials,

172   'Deriving the rate laws for *PER* transcription'). The parameter φ represents the gene dosage of

173   *PER*, relative to homozygous diploid, $\varphi = 1$. For cells over- (or under-) expressing the *PER* gene, φ

174   > 1 (or $\varphi < 1$). The expression for A_{free} in Eq. (13) is derived by solving the condition for equilibrium

175   binding of BMAL:CLOCK (A) and PER:CRY (P) to form an inactive complex (C); namely, $K_d C =$

176     $A_{free} P_{free}$, where $A_{free} = A_T - C$ and $P_{free} = P - C$.

177   The KF equations (10)-(13) are written in dimensionless form; in particular, $t = \beta \times$ time, where β

178   is the first-order rate constant (h^{-1}) for removal of all three species in Eqs. (10)-(12). Furthermore,

179   P, K_d, A_T and A_{free} are all scaled by the same factor, $P^* \approx 25$ nM (Supplementary Materials,

180   'Estimation of the scaling factor P^*').

181   Notice that, in the KF model, nonlinearity in the transcription term is due to tight stoichiometric

182   binding between PER:CRY and BMAL:CLOCK, not (as in Goodwin's equations) to cooperative

183   participation of nuclear PER in the regulation of *PER* gene expression. Consequently, the KF model

10

184   circumvents the unreasonable cooperativity constraint ($p > 8$) of Goodwin's model. (Don't

185   confuse the Hill exponent, p, in Goodwin's model with the concentration of nuclear PER, P, in the

186   KF model.)

187   In addition to the SNF model, Kim & Forger proposed two extended models, in which the core

188   negative feedback loop involving PER and BMAL is supplemented with (either) an additional

189   <u>negative</u> feedback from REV-ERB on transcription of the *BMAL1* gene (called the NNF model,

190   Figure 2b) (or) an additional <u>positive</u> feedback from ROR on transcription of the *BMAL1* gene

191   (called the PNF model, Figure 2c). Both the NNF and PNF models include the ODEs of the core

192   SNF model.

193   <u>Kim-Forger NNF Model</u>. Equations (10)-(13), plus

$$\frac{dV}{dt} = \frac{A_{\text{free}}}{A_T} - \delta V \tag{14}$$

$$\frac{dA_T}{dt} = \frac{\gamma}{V} - \delta A_T \tag{15}$$

194

195   where V is the (scaled) concentration of REV-ERB, γ is a rate constant for *BMAL1* transcription,

196   and δ is a rate constant that sets the time scale for the feedback loop.

197   <u>Kim-Forger PNF Model</u>. Equations (10)-(13), plus

$$\frac{dR}{dt} = \frac{A_{\text{free}}}{A_T} - \delta R \tag{16}$$

$$\frac{dA_T}{dt} = \gamma R - \delta A_T \qquad (17)$$

198 where R is the (scaled) concentration of ROR, and γ and δ are defined similarly as in the NNF

199 equations.

200 In Tables S1 and S2 we provide definitions of all the variables and kinetic constants in these

201 models.

202 While the KF models appear to oscillate robustly and avoid Goodwin's unrealistic constraint ($p >$

203 8), the core SNF model seems to have an unreasonable constraint of its own; namely, the

204 maximum permissible value of the dissociation constant of the nuclear PER:BMAL complex is K_d

205 $= 10^{-4}$, which is orders of magnitude too small for protein-protein binding. To see why, we

206 convert KF's dimensionless K_d into its dimensional form, $K_d < 10^{-3}$ nM, by multiplying by $P^* \approx 10$

207 nM (this is an order-of-magnitude estimate). Because the time constant for dissociation of the

208 PER:BMAL complex is expected to be on the order of minutes (i.e., $k_{\text{unbind}} \approx 0.01 \text{ s}^{-1}$), the

209 binding constant for the complex would have to be $k_{\text{bind}} = \frac{k_{\text{unbind}}}{K_d} \approx \frac{0.01 \text{ s}^{-1}}{0.001 \text{ nM}} = 10 \text{ nM}^{-1}\text{s}^{-1} =$

210 $10^{10} \text{ M}^{-1}\text{s}^{-1}$. However, protein-protein binding rate constants are typically on the order of 10^6

211 $\text{M}^{-1}\text{s}^{-1}$ (40). So, a physically realistic value for the dissociation constant of the PER:BMAL complex

212 is $K_d \approx 10$ nM, or in dimensionless terms, $K_d \approx 1$. Even if the binding is especially tight, K_d should

213 be at least on the order of 0.1. In fact, Fribourgh et al. (41), who recently studied the docking of

214 PER2:CRY1/2 to the core PAS domain of BMAL:CLOCK, measured $K_d \approx 400$ nM, or in dimensionless

215 terms, $K_d \approx 40$. This estimate may easily be off by a factor of 10, because the measurements were

216 made *in vitro* with purified protein domains (not with full length proteins). Nonetheless,

12

217   comparing our theoretical estimate and this experimental result, we might conclude that $K_d \approx$

218   0.1—10, in dimensionless terms.

219   Hence, KF's dissociation constant is unrealistically small by several orders of magnitude. In this

220   work we consider some realistic changes to the SNF model that will increase the robustness of

221   its oscillations. In the process, we come up with some other surprising reassessments of the KF

222   model.

223   **RESULTS AND DISCUSSION**

224   **Longer Feedback Loop and Saturating PER Degradation Increase the Oscillatory Robustness of**

225   **the Kim-Forger SNF Model.**

226   Our primary goal in modifying KF models is to alleviate the unreasonable constraint on K_d, the

227   dissociation constant of the PER:BMAL complex. To this end, we considered the same two

228   changes that were made to Goodwin's model to increase its robustness: first, increasing the

229   number of dynamical species in the PER-BMAL negative feedback loop, and second, introducing

230   a Michaelis-Menten rate law for the degradation of nuclear PER.

231   Longer feedback loop. Given that PER has 10-20 phosphorylation sites (35), it is reasonable to

232   assume that cytoplasmic PER is phosphorylated sequentially on 1, …, n-3 sites before it is

233   transported into the nucleus. Hence, we rewrite P_C as P_0 and insert between Eq. (11) and Eq. (12)

234   a sequence of linear ODEs for the intermediate (phosphorylated) states, P_1, …, P_{n-3}. This change

235   lengthens the time between *PER* mRNA transcription and the negative feedback signal generated

236   by nuclear PER and consequently increases the oscillatory potential of the negative feedback loop

237   (42).

13

238   <u>Saturating degradation of nuclear PER</u>. PER is degraded by proteasomes after it is poly-

239   ubiquitinated by the E3 ligase β-Trcp (43). Because the rate of this enzyme-mediated reaction

240   likely saturates at large substrate concentration, it is reasonable to replace the linear kinetics for

241   nuclear PER degradation in Eq. (12) by a Michaelis-Menten rate law (43),

$$\frac{dP}{dt} = P_c - \frac{\beta K_{\mathrm{m}} P}{K_{\mathrm{m}} + P} \tag{18}$$

242

243   In Eq. (18), K_{m} is the Michaelis constant of the rate law and βK_{m} is the 'V_{max}'. This change also has

244   the potential to increase the oscillatory robustness of the model. Intuitively, the upper limit to

245   the rate of PER degradation introduced by the Michaelis-Menten rate law causes nuclear PER

246   concentration to react sluggishly to changes in the rate of *PER* mRNA production, which is

247   another sort of 'lag' in the negative feedback loop.

248   Both modifications indeed improve the robustness of oscillations in the SNF model. 'Longer

249   feedback loops' (with no other modifications of the SNF model) can increase by a hundred fold

250   the maximum K_{d} for oscillations, as shown in Figure 3a. This upper bound is still below the range

251   of physical acceptability. If we introduce both 'saturating degradation' and an '*n*-component

252   feedback loop', then the maximum K_{d} for oscillations increases to a value of 1 (see Figure S1), but

253   this happy result is suspect because the doubly-modified SNF model exhibits oscillations even as

254     $A_T \to 0$ when $n \geq 4$. This result is impossible because there can be no expression of the *PER* gene

255   when BMAL concentration is zero. The problem, of course, is that the rate law for *PER*

256   transcription (rate $\propto A_{\mathrm{free}}/A_{\mathrm{T}}$) is valid only if BMAL saturates the *PER* E-boxes. To get around this

257   restriction, we consider some other potential rate laws for *PER* gene transcription (see

258   Supplementary Materials, 'Deriving the rate laws for *PER* transcription').

259   **Modifying the *PER* Transcription Rate Law Increases the Robustness of the SNF Model Still**

260   **Further.**

261   We consider two slightly different rate laws to replace the KF expression for the rate of *PER* gene

262   transcription:

Rate Law 0:
$$\frac{dM}{dt} = \varphi \frac{A_{\text{free}}}{A_{\text{T}}} - M \tag{19-0}$$

Rate Law 1:
$$\frac{dM}{dt} = \varphi \frac{A_{\text{free}}}{K_{\text{A}} + A_{\text{T}}} - M \tag{19-1}$$

Rate Law 2:
$$\frac{dM}{dt} = \varphi \frac{A_{\text{free}}}{K_{\text{A}} + A_{\text{free}}} - M \tag{19-2}$$

263

264   Rate law 0 is, of course, the original KF expression. When $A_{\text{free}} = A_{\text{T}}$, the maximum rate of

265   transcription is φ. (In our scaling of the differential equations, the maximum rate of transcription

266   of *PER* mRNA = φ = 1 for WT homozygous diploid cells, and the rate increases or decreases with

267   φ for cells over- or under-expressing *PER* mRNA, either by manipulating *PER* gene dosage or the

268   strength of the *PER* gene promoter.) For rate laws 1 and 2, the maximum rate of transcription is

269    $\varphi \frac{A_{\text{T}}}{K_{\text{A}} + A_{\text{T}}}$, i.e., the maximum rate depends on how strongly BMAL:CLOCK binds to the E-box,

270   characterized by the dissociation constant K_{A}. Rate laws 1 and 2 also imply that the transcription

271   rate is proportional to A_{free} (not $A_{\text{free}} / A_{\text{T}}$) when A_{T} becomes small. These three rate laws

272   represent different limiting cases of BMAL:CLOCK binding to E-boxes, as explained in detail in the

273   Supplementary Materials, 'Deriving the rate laws for *PER* transcription'. Recall that the KF rate

15

274   law 0 applies to the case in which binding between PER:CRY and BMAL:CLOCK is independent of

275   the binding between BMAL:CLOCK and E-box, and BMAL:CLOCK complexes saturate *PER* E-boxes.

276   Rate law 1 is a slight modification of the KF rate law 0, relaxing the saturation of *PER* E-boxes by

277   BMAL:CLOCK. Finally, rate law 2 is based on a different model of the regulation of *PER*

278   transcription, where PER:CRY binds tightly to BMAL:CLOCK, and only the free form of

279   BMAL:CLOCK binds to the E-box.

280   **Modified Kim-Forger SNF equations.** Taking all of the aforementioned changes into account,

281   we have:

$$\frac{dM}{dt} = \varphi \cdot F(A_{\text{free}}) - M \tag{20}$$

$$\frac{dP_0}{dt} = M - P_0 \tag{21}$$

$$\frac{dP_i}{dt} = P_{i-1} - P_i, \quad i = 1, \dots, n-3 \tag{22}$$

$$\frac{dP}{dt} = P_{n-3} - G(P) \tag{23}$$

$$A_{\text{free}} = \frac{1}{2}\left[A_{\text{T}} - P - K_{\text{d}} + \sqrt{(A_{\text{T}} - P - K_{\text{d}})^2 + 4K_{\text{d}}A_{\text{T}}}\right] \tag{24}$$

282

283   where $F(A_{\text{free}}) = \begin{cases} A_{\text{free}}/A_{\text{T}} \\ A_{\text{free}}/(K_{\text{A}} + A_{\text{T}}) \\ A_{\text{free}}/(K_{\text{A}} + A_{\text{free}}) \end{cases}$, and $G(P) = \begin{cases} P \\ \beta K_{\text{m}} P/(K_{\text{m}} + P) \end{cases}$.

284   To keep track of all these different versions, we introduce the notation SNF(TDN), where T

285   denotes the *PER* transcription rate law (0, 1 or 2), D denotes the PER degradation rate law (L for

286   'linear' or M for Michaelian), and N denotes the number of species in the negative feedback loop

287   (Supplementary Materials, 'Model naming convention'). For example, the original KF SNF model

288   is denoted SNF(0L3).

289   We have already shown the two-parameter bifurcation diagram (log K_d versus log A_T) for

290   SNF(0LN) in Figure 3a. The corresponding bifurcation diagram for SNF(1MN), Figure 3b, shows

291   that our extension of the SNF model (with modified transcription rate and saturating degradation

292   of nuclear PER) is more robust than the original KF model in that oscillations are now possible for

293   K_d as large as 1. In Figures 3c and d, we display the matching bifurcation diagrams for SNF(2LN)

294   and SNF(2MN), respectively. Again, we see that saturating degradation of nuclear PER is crucial

295   for permitting oscillations for $K_d > 0.01$. Comparing Figure 3b and 3d, we see that transcription

296   rate law 1 generates more robust oscillations than rate law 2 for K_d values larger than 0.1, but

297   rate law 2 is more robust for N = 3.

298   **An Additional Positive Feedback Loop Involving ROR Increases the Domain of Oscillations.**

299   Next, we explore Kim & Forger's NNF and PNF models (above), with modified rate laws for gene

300   transcription. For the rates of transcription of *PER*, *REV-ERB* and *ROR* genes, we use Rate Law 2,

301   Eq. (19-0), and for the transcriptional activation and repression of the *BMAL* gene by ROR

302   (variable R) and REV-ERB (variable V), we replace the functions γR and γ/V (as originally proposed

303   by Kim & Forger) by $A_{MAX} \cdot R/(R+1)$ and $A_{MAX}/(V+1)$, respectively. The new rate laws assume that

304   R and V are scaled by the dissociation constants of these proteins with the promoter of the *BMAL*

17

305   gene. These new rate laws remedy an issue in KF's original PNF and NNF models, for which the

306   rate of BMAL synthesis does not saturate as $R \to \infty$ or $V \to 0$.

307   **Modified Kim-Forger NNF model.** Equations (20)-(24) with $F(A_{\text{free}}) = A_{\text{free}}/(K_A + A_{\text{free}})$ plus

$$\frac{dA_T}{dt} = \delta\left[A_{\text{MAX}}\frac{1}{V+1} - A_T\right] \tag{25}$$

$$\frac{dV}{dt} = \delta\left[V_{\text{MAX}}\frac{A_{\text{free}}}{A_{\text{free}} + K_A} - V\right] \tag{26}$$

308

309   **Modified Kim-Forger PNF model.** Equations (20)-(24) with $F(A_{\text{free}}) = A_{\text{free}}/(K_A + A_{\text{free}})$ plus

$$\frac{dA_T}{dt} = \delta\left[A_{\text{MAX}}\frac{R}{R+1} - A_T\right] \tag{27}$$

$$\frac{dR}{dt} = \delta\left[R_{\text{MAX}}\frac{A_{\text{free}}}{A_{\text{free}} + K_A} - R\right] \tag{28}$$

310

311   Finally, in wild-type SCN cells, nuclear REV-ERB and ROR compete for binding to the *BMAL*

312   promoter. So, it is reasonable to consider a model that accounts for the effects of REV-ERB and

313   ROR together. (This case was not considered by Kim and Forger.) In the new model (PNNF) the

314   BMAL synthesis term accounts for competitive regulation by both REV-ERB and ROR, and also

315   features a basal synthesis rate (ε) for the case when R and V are both zero. The PNNF model

316   assumes that REV-ERB and ROR bind to the *BMAL* promoter with the same affinity.

317   **PNNF equations.** Equations (20)-(24) with $F(A_{\text{free}}) = A_{\text{free}}/(K_A + A_{\text{free}})$ plus

$$\frac{dA_T}{dt} = \delta \left[A_{\text{MAX}} \frac{\varepsilon + R}{1 + V + R} - A_T \right] \tag{29}$$

$$\frac{dR}{dt} = \delta \left[R_{\text{MAX}} \frac{A_{\text{free}}}{A_{\text{free}} + K_A} - R \right] \tag{30}$$

$$\frac{dV}{dt} = \delta \left[V_{\text{MAX}} \frac{A_{\text{free}}}{A_{\text{free}} + K_A} - V \right] \tag{31}$$

318

319   The original KF models (SNF, NNF, and PNF) were compared to each other by plotting the regions

320   where each model oscillates with respect to fold changes in *BMAL* and *PER* transcription rates,

321   Figure 4a, which is identical to Figure 5a in the Kim-Forger paper (27). The major conclusion from

322   Kim & Forger's calculations was that the additional negative feedback loop increases oscillatory

323   robustness of the model while the additional positive feedback loop decreases oscillatory

324   robustness.

325   After our modifications, the models show quite different behavior (Figure 4b). (In comparing

326   Figures 4a and b, keep in mind that $K_d = 10^{-5}$ in panel a (the KF value) but $K_d = 10^{-1}$ (more realistic

327   value) in panel b.) In panel b, it is evident that the stoichiometric balance between PER and BMAL

328   required for oscillations in the KF models is not preserved in our models, which is due to the

329   introduction of the Michaelis-Menten rate law for degradation of nuclear PER, as suggested by

330   Figure S2. Furthermore, in our modified models, the NNF and SNF regions of oscillation are

331   approximately equal, implying that the additional negative feedback loop is not having much of

332   an effect on the system's behavior. Kim and Forger concluded that the additional negative

333   feedback through REV-ERB must be slow compared to the core negative feedback loop in order

19

334   to provide a robustness benefit to the SNF loop (27). However, in our version of the models, it

335   appears that neither increasing the length of the REV-ERB feedback loop (Figure S3a) nor

336   decreasing the time scaling factor δ (Figure S3b) changes the NNF model's robustness. Thus, in

337   the modified models, the role of the auxiliary negative feedback loop is unclear. Lastly, in our

338   implementation, the PNF model has by far the largest region of oscillations, and the PNNF model

339   shares characteristics of the NNF and PNF models.

340   **All Four Models (SNF, NNF, PNF and PNNF) Have Comparable Robustness with Respect to ~24**

341   **Hour Oscillations.**

342   In the previous subsection, we were concerned only with the existence of oscillations and not

343   with their periods. Figure 5 redraws the bifurcation plots in Figure 4b with colors to indicate the

344   oscillatory periods. (To convert from dimensionless period τ to period in hours, we assume that

345     $\beta_1 = 1 \text{ h}^{-1}$, which makes the period of SNF(2M8) model with its default parameter values (Table

346   S4) around 24 h (Figure S5).) The oscillatory period for each model varies over characteristic

347   ranges. The modified SNF and NNF models have nearly identical period distributions over a range

348   of $16 - 26$ h, supporting our conclusion that the additional negative feedback loop has little effect

349   on the system's periodicity. The PNF and PNNF models have broader period distributions: $15 -$

350   45 h and $16 - 39$ h, respectively, confirming the common understanding that a combination of

351   positive and negative feedback loops generates robust oscillations over a broad range of periods

352   (42, 44). Nonetheless, Figure 5 also indicates that all four modified models exhibit similar bands

353   of circadian periodicity ($23 - 25$ h). So, while the PNF model has a much larger oscillatory domain

354   than the other models, much of this area corresponds to non-circadian periods.

355   Finally, we note that the PNF(2M8) model exhibits subcritical Hopf bifurcations, which expand

356   the region of long-period (> 40 h) oscillations, as shown in Figure S4.

357   **CONCLUSION**

358   The Kim-Forger (KF) models of mammalian circadian rhythms (called SNF, NNF and PNF) are

359   appealing in many respects; but they rely on an unrealistic requirement for oscillations, namely

360   that the equilibrium dissociation constant of the PER:CRY::BMAL:CLOCK complex must be K_d <

361   10^{-3} nM, which is orders of magnitude smaller than a reasonable value for protein-protein

362   interactions ($K_d \approx$ 1—100 nM). This difficulty can be ameliorated (1) by lengthening the core

363   negative feedback loop between *PER* mRNA transcription and PER:CRY inactivation of

364   BMAL:CLOCK (the transcription factor driving *PER* expression), and/or (2) by implementing a

365   Michaelis-Menten rate law for the degradation of nuclear PER. The KF models were further

366   modified by introducing alternative rate laws for BMAL:CLOCK-mediated transcription of clock

367   genes (*PER*, *REV-ERB* and *ROR*) to correct a problem at low expression of the *BMAL* gene, and to

368   provide more accurate rate laws for the effects of REV-ERB and ROR on *BMAL* expression.

369   With these modifications, we find (Figure 3b) that the SNF model can exhibit oscillations for K_d

370   as large as 25 nM for 0.05 nM < A_T < 50 nM. These values are consistent with experimental

371   measurements of *in vitro* binding between PER:CRY and BMAL (41) and of the total number of

372   BMAL and CLOCK molecules in mouse cells (45).

373   The simple negative feedback loop (SNF), whereby PER inhibits its own synthesis, can be

374   supplemented with an auxiliary positive feedback from ROR (PNF) or a negative feedback from

375   REV-ERB (NNF) on the synthesis of BMAL. A fourth model (PNNF) considers all three feedback

376   loops together. The behaviors of our modified models differ significantly from Kim and Forger's

377   original conclusions. Kim and Forger's observation of a stoichiometric balance between PER and

378   BMAL was not observed in the modified models. The modified models also do not share the same

379   trends in robustness (in terms of the size of the oscillatory domain in parameter space). In the

380   original KF models, NNF was the most robust model and PNF the least, but in our modified

381   models, PNF was considerably more robust than the other three models. Nonetheless, the

382   domains of circadian oscillations (23-25 h) are quite comparable for all four of our models. Since

383   the auxiliary positive and negative feedback loops do not seem to provide any additional

384   circadian robustness to the simple negative feedback loop, the functions of ROR and REV-ERB in

385   generating circadian rhythmicity are still unclear in our versions of the KF models.

386   We propose that these models can be extended in future publications to explore other known

387   behaviors of the mammalian circadian clock. For instance, our models do not address the

388   circadian clock's temperature-compensation or phase-shifting properties. Adding these key

389   features may answer some remaining questions about the behaviors of these models. For

390   example, the additional negative feedback loop between REV-ERB and BMAL may contribute to

391   these features. Another question that could be addressed with these models is the function of

392   an anti-sense transcript of the PER2 gene (46). Furthermore, these models could be applied in

393   chronotherapy and chrono-pharmacology studies. One such application would be modeling

394   PER2's interaction with the tumor suppressor protein p53 in stressed (e.g., DNA damage) cells

395   compared to un-stressed cells (47, 48).

396   **Acknowledgements**

22

REFERENCES

1. Patke A, Young MW, Axelrod S. Molecular mechanisms and physiological importance of circadian rhythms. Nature reviews Molecular cell biology. 2020;21(2):67-84.

2. Pittendrigh CS. Circadian rhythms and the circadian organization of living systems. Cold Spring Harbor symposia on quantitative biology. 1960;25:159-84.

3. Kurosawa G, Iwasa Y. Temperature compensation in circadian clock models. Journal of theoretical biology. 2005;233(4):453-68.

4. Kidd PB, Young MW, Siggia ED. Temperature compensation and temperature sensation in the circadian clock. Proceedings of the National Academy of Sciences of the United States of America. 2015;112(46):E6284-92.

5. Ruoff P, Rensing L, Kommedal R, Mohsenzadeh S. Modeling temperature compensation in chemical and biological oscillators. Chronobiol Int. 1997;14(5):499-510.

6. Gupta A, Hepp B, Khammash M. Noise Induces the Population-Level Entrainment of Incoherent, Uncoupled Intracellular Oscillators. Cell Syst. 2016;3(6):521-31 e13.

7. Aschoff J, Pohl H. Phase relations between a circadian rhythm and its zeitgeber within the range of entrainment. Naturwissenschaften. 1978;65(2):80-4.

8. Redfern P, Minors D, Waterhouse J. Circadian rhythms, jet lag, and chronobiotics: an overview. Chronobiol Int. 1994;11(4):253-65.

9. Partch CL, Green CB, Takahashi JS. Molecular architecture of the mammalian circadian clock. Trends in cell biology. 2014;24(2):90-9.

10. Zhang EE, Kay SA. Clocks not winding down: unravelling circadian networks. Nature reviews Molecular cell biology. 2010;11(11):764-76.

11. Takahashi JS. Molecular components of the circadian clock in mammals. Diabetes Obes Metab. 2015;17 Suppl 1:6-11.

12. Smolen P, Byrne JH. Circadian Rhythm Models. In: Squire LR, editor. Encyclopedia of Neuroscience: Oxford: Academic Press; 2009. p. 957-63.

13. Trott AJ, Menet JS. Regulation of circadian clock transcriptional output by CLOCK:BMAL1. PLoS genetics. 2018;14(1):e1007156.

14. Zhang R, Lahens NF, Ballance HI, Hughes ME, Hogenesch JB. A circadian gene expression atlas in mammals: Implications for biology and medicine. Proceedings of the National Academy of Sciences of the United States of America. 2014;111(45):16219-24.

15. Yeung J, Mermet J, Jouffe C, Marquis J, Charpagne A, Gachon F, et al. Transcription factor activity rhythms and tissue-specific chromatin interactions explain circadian gene expression across organs. Genome research. 2018;28(2):182-91.

16. Pavlidis T. A model for circadian clocks. Bull Math Biophys. 1967;29(4):781-91.

17. Goldbeter A. A model for circadian oscillations in the Drosophila period protein (PER). Proc R Soc Lond B. 1995;261(1362):319-24.

18. Leloup JC, Goldbeter A. Toward a detailed computational model for the mammalian circadian clock. Proceedings of the National Academy of Sciences of the United States of America. 2003;100(12):7051-6.

19. Ueda HR, Hagiwara M, Kitano H. Robust oscillations within the interlocked feedback model of Drosophila circadian rhythm. Journal of theoretical biology. 2001;210(4):401-6.

20. Gonze D. Modeling circadian clocks: From equations to oscillations. Cent Eur J Biol. 2011;6(5):699-711.

21. Goodwin BC. Oscillatory behavior in enzymatic control processes. Adv Enzyme Regul. 1965;3:425-38.

22. Goodwin BC. An entrainment model for timed enzyme syntheses in bacteria. Nature. 1966;209(5022):479-81.

23. Ruoff P, Rensing L. The temperature-compensated goodwin model simulates many circadian clock properties. Journal of theoretical biology. 1996;179(4):275-85.

24. Ruoff P, Vinsjevik M, Monnerjahn C, Rensing L. The Goodwin oscillator: On the importance of degradation reactions in the circadian clock. J Biol Rhythm. 1999;14(6):469-79.

25. Ruoff P, Vinsjevik M, Monnerjahn C, Rensing L. The Goodwin model: Simulating the effect of light pulses on the circadian sporulation rhythm of Neurospora Crassa. Journal of theoretical biology. 2001;209(1):29-42.

26. Relogio A, Westermark PO, Wallach T, Schellenberg K, Kramer A, Herzel H. Tuning the Mammalian Circadian Clock: Robust Synergy of Two Loops. PLoS computational biology. 2011;7(12).

27. Kim JK, Forger DB. A mechanism for robust circadian timekeeping via stoichiometric balance. Molecular systems biology. 2012;8:630.

28. Mirsky HP, Liu AC, Welsh DK, Kay SA, Doyle FJ, 3rd. A model of the cell-autonomous mammalian circadian clock. Proceedings of the National Academy of Sciences of the United States of America. 2009;106(27):11107-12.

29. Kim JK. Protein sequestration versus Hill-type repression in circadian clock models. Iet Syst Biol. 2016;10(4):125-35.

30. Masters M, Donachie WD. Repression and the control of cyclic enzyme synthesis in Bacillus subtilis. Nature. 1966;209(5022):476-9.

31. Tyson JJ, Othmer HG. The Dynamics of Feedback Control Circuits in Biochemical Pathways. Progress in Theoretical Biology: Elsevier; 1978. p. 1-62.

32. Rapp P. Analysis of Biochemical Phase-Shift Oscillators by a Harmonic Balancing Technique. J Math Biol. 1976;3(3-4):203-24.

33. Griffith JS. Mathematics of cellular control processes. I. Negative feedback to one gene. Journal of theoretical biology. 1968;20(2):202-8.

34. Gonze D, Abou-Jaoude W. The Goodwin model: behind the Hill function. PLoS One. 2013;8(8):e69573.

35. Vanselow K, Vanselow JT, Westermark PO, Reischl S, Maier B, Korte T, et al. Differential effects of PER2 phosphorylation: molecular basis for the human familial advanced sleep phase syndrome (FASPS). Genes & development. 2006;20(19):2660-72.

36. MacDonald N. Time Lags in Biological Models. 1 ed: Springer-Verlag Berlin Heidelberg; 1978. VIII, 114 p.

37. Bliss RD, Painter PR, Marr AG. Role of feedback inhibition in stabilizing the classical operon. Journal of theoretical biology. 1982;97(2):177-93.

38. Kurosawa G, Iwasa Y. Saturation of enzyme kinetics in circadian clock models. J Biol Rhythms. 2002;17(6):568-77.

39. Gonze D, Bernard S, Waltermann C, Kramer A, Herzel H. Spontaneous synchronization of coupled circadian oscillators. Biophysical journal. 2005;89(1):120-9.

485 40. Northrup SH, Erickson HP. Kinetics of protein-protein association explained by Brownian
486   dynamics computer simulation. Proceedings of the National Academy of Sciences of the United
487   States of America. 1992;89(8):3338-42.

488 41. Fribourgh JL, Srivastava A, Sandate CR, Michael AK, Hsu PL, Rakers C, et al. Dynamics at the
489   serine loop underlie differential affinity of cryptochromes for CLOCK:BMAL1 to control circadian
490   timing. eLife. 2020;9.

491 42. Novak B, Tyson JJ. Design principles of biochemical oscillators. Nature reviews Molecular cell
492   biology. 2008;9(12):981-91.

493 43. D'Alessandro M, Beesley S, Kim JK, Jones Z, Chen R, Wi J, et al. Stability of Wake-Sleep Cycles
494   Requires Robust Degradation of the PERIOD Protein. Current biology : CB. 2017;27(22):3454-67
495   e8.

496 44. Tsai TY, Choi YS, Ma W, Pomerening JR, Tang C, Ferrell JE, Jr. Robust, tunable biological
497   oscillations from interlinked positive and negative feedback loops. Science. 2008;321(5885):126-
498   9.

499 45. Narumi R, Shimizu Y, Ukai-Tadenuma M, Ode KL, Kanda GN, Shinohara Y, et al. Mass
500   spectrometry-based absolute quantification reveals rhythmic variation of mouse circadian clock
501   proteins. Proceedings of the National Academy of Sciences of the United States of America.
502   2016;113(24):E3461-E7.

503 46. Koike N, Yoo SH, Huang HC, Kumar V, Lee C, Kim TK, et al. Transcriptional architecture and
504   chromatin landscape of the core circadian clock in mammals. Science. 2012;338(6105):349-54.

505 47. Gotoh T, Kim JK, Liu J, Vila-Caballer M, Stauffer PE, Tyson JJ, et al. Model-driven experimental
506   approach reveals the complex regulatory distribution of p53 by the circadian factor Period 2.
507   Proceedings of the National Academy of Sciences of the United States of America.
508   2016;113(47):13516-21.

509 48. Zou XL, Kim DW, Gotoh T, Liu JJ, Kim JK, Finkielstein CV. A Systems Biology Approach Identifies
510   Hidden Regulatory Connections Between the Circadian and Cell-Cycle Checkpoints. Front
511   Physiol. 2020;11.

512
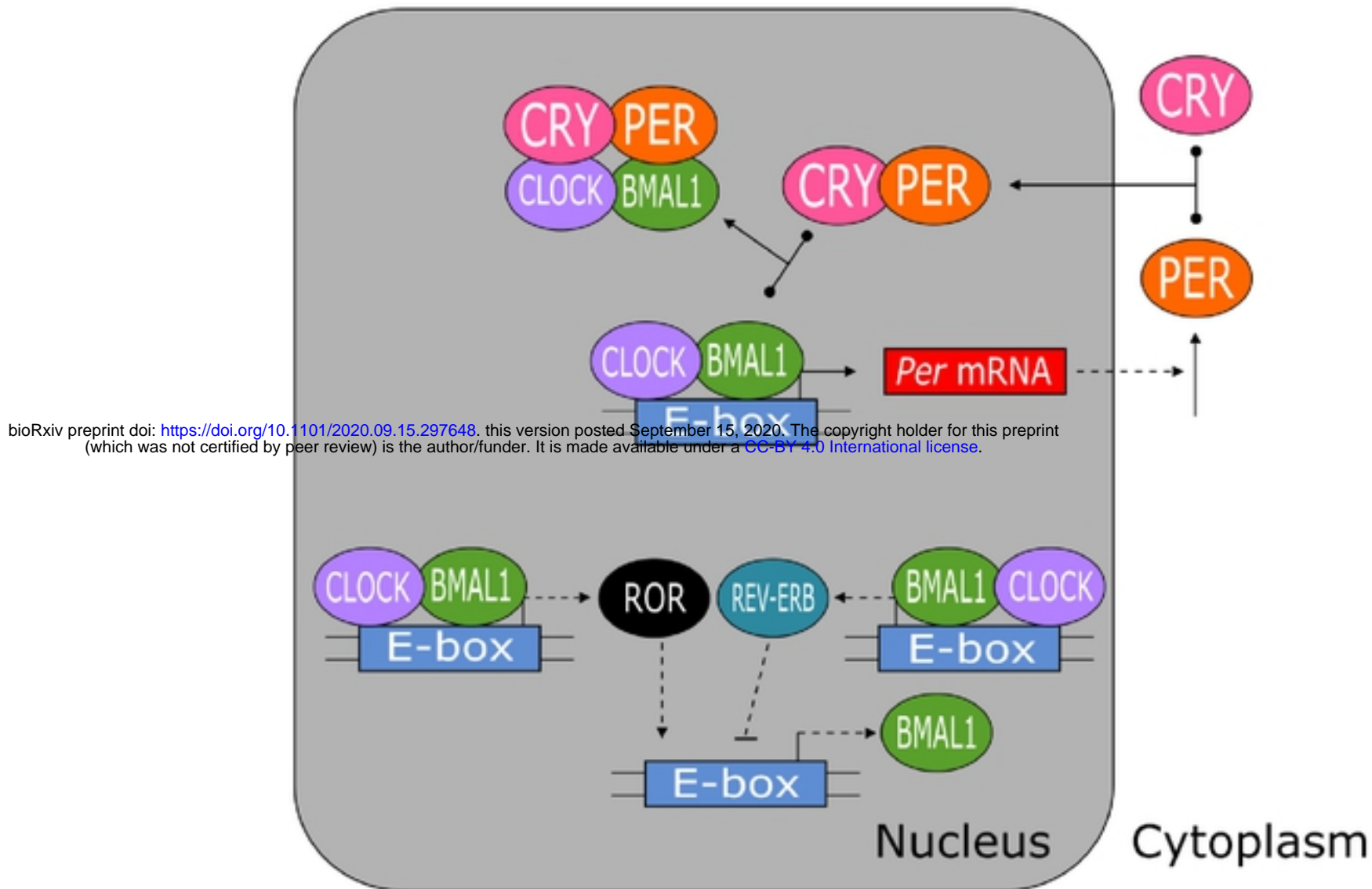
FIGURES

Figure 1. Three major feedback loops regulate the mammalian circadian clock. The core negative feedback loop is between PER:CRY and BMAL1:CLOCK. The two sources of additional feedback are negative feedback between REV-ERB and BMAL1 and positive feedback between ROR and BMAL1. PER1/2, CRY1/2, and RORα/β are simplified to PER, CRY, and ROR, respectively. Solid lines indicate chemical reactions; the T-shaped reactions indicate reversible binding of proteins to form multicomponent complexes. Dashed lines indicate regulatory signals (positive regulation = barbed arrow, and negative regulation = blunt arrow).
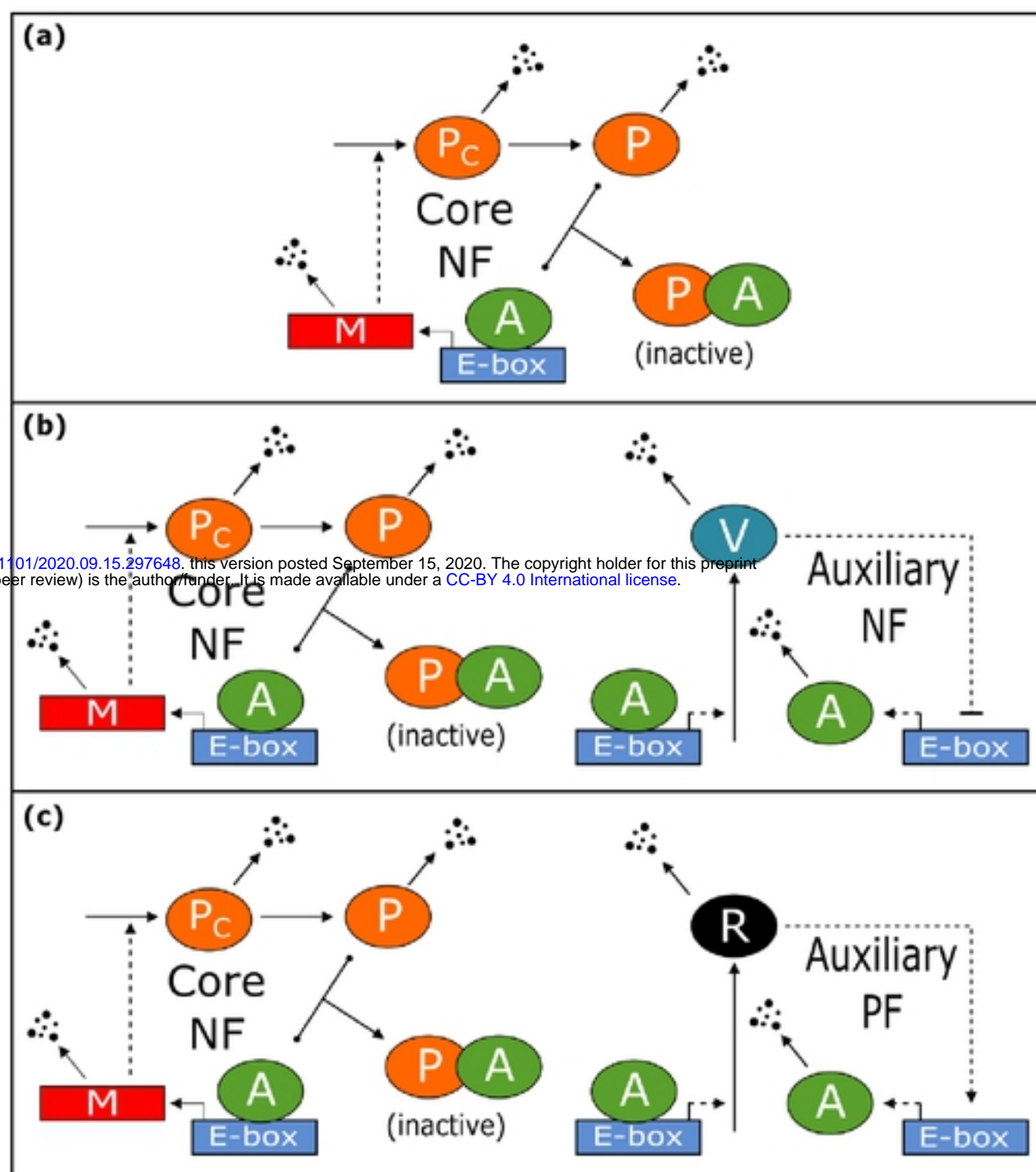
Figure 2. Wiring diagrams for the three Kim-Forger models: SNF **(a)**, NNF **(b)**, and PNF **(c)**. To simplify the models, several molecular species that do not contribute significantly to the feedback loops are not explicitly represented. For example, in the SNF loop, CLOCK and CRY are not shown. In the NNF and PNF loops, mRNAs encoding REV-ERB, ROR and BMAL are not shown, nor are the cytoplasmic forms of these proteins. Solid and dashed lines indicate reactions and regulations, as in Figure 1.
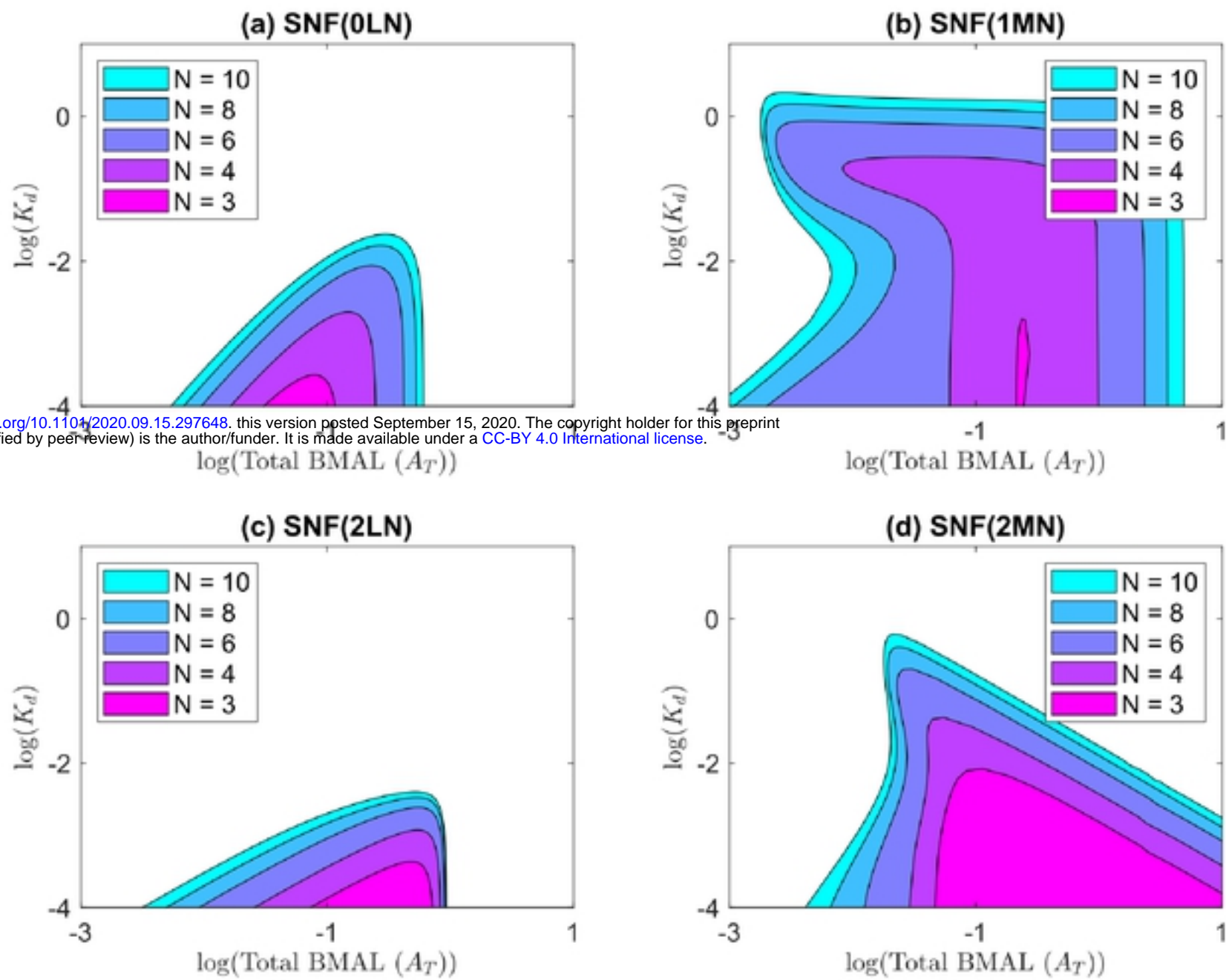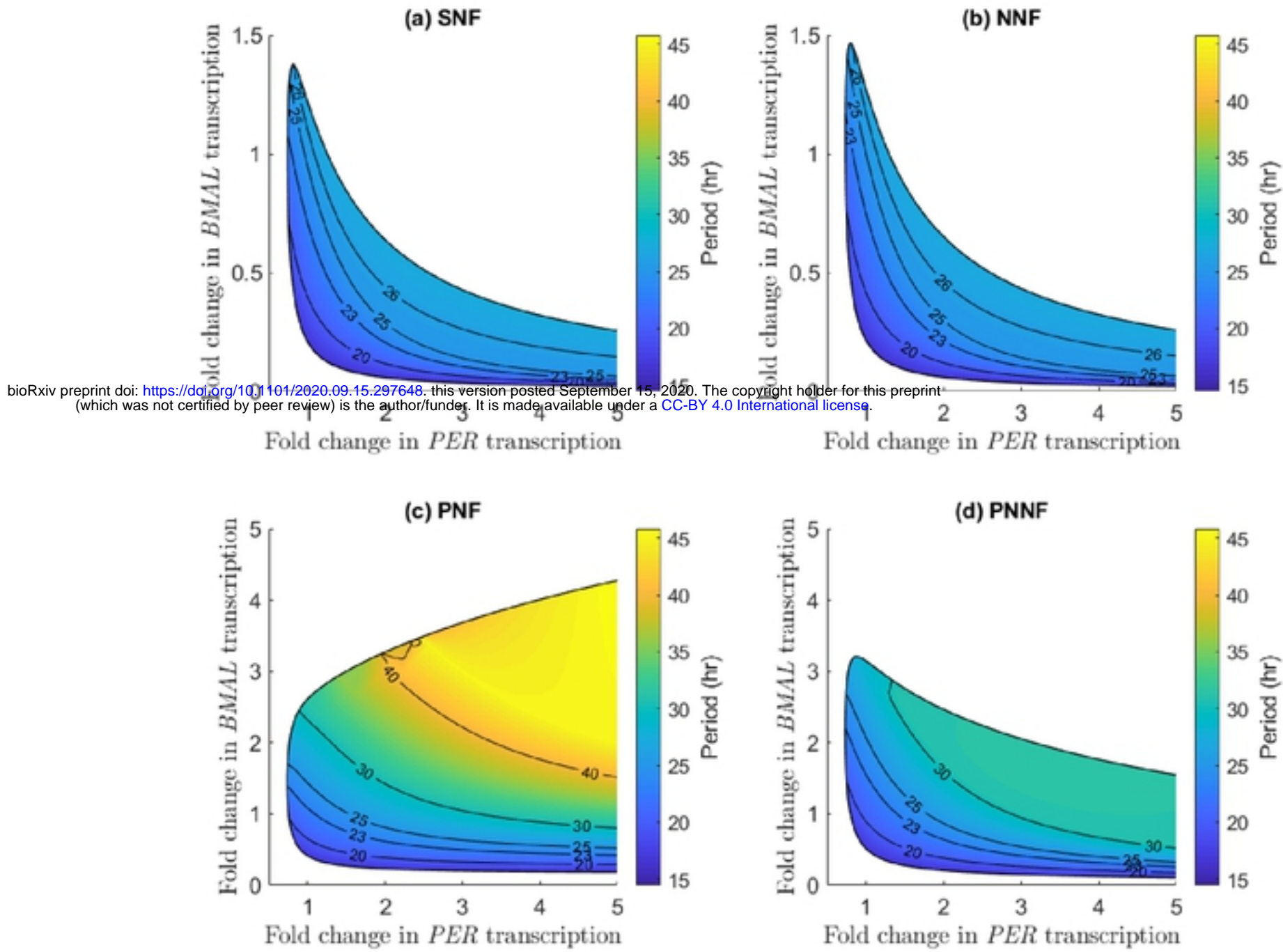
Figure 3. Two-parameter bifurcation diagrams, with respect to K_d and A_T. **(a)** The original KF SNF(0LN) model, with linear rate of degradation of nuclear PER. **(b)** SNF(1MN) model, with Michaelis-Menten degradation of nuclear PER. **(c)** SNF(2LN) model, with rate law 2 for *PER* mRNA transcription and linear degradation of nuclear PER. **(d)** SNF(2MN) model, with rate law 2 for *PER* mRNA transcription and Michaelis-Menten degradation of nuclear PER. Only model SNF(1MN) admits oscillations for reasonable values of $K_d \approx 1$. The parameter values used in these calculations are provided in Table S3; in particular, $\varphi = 1$.
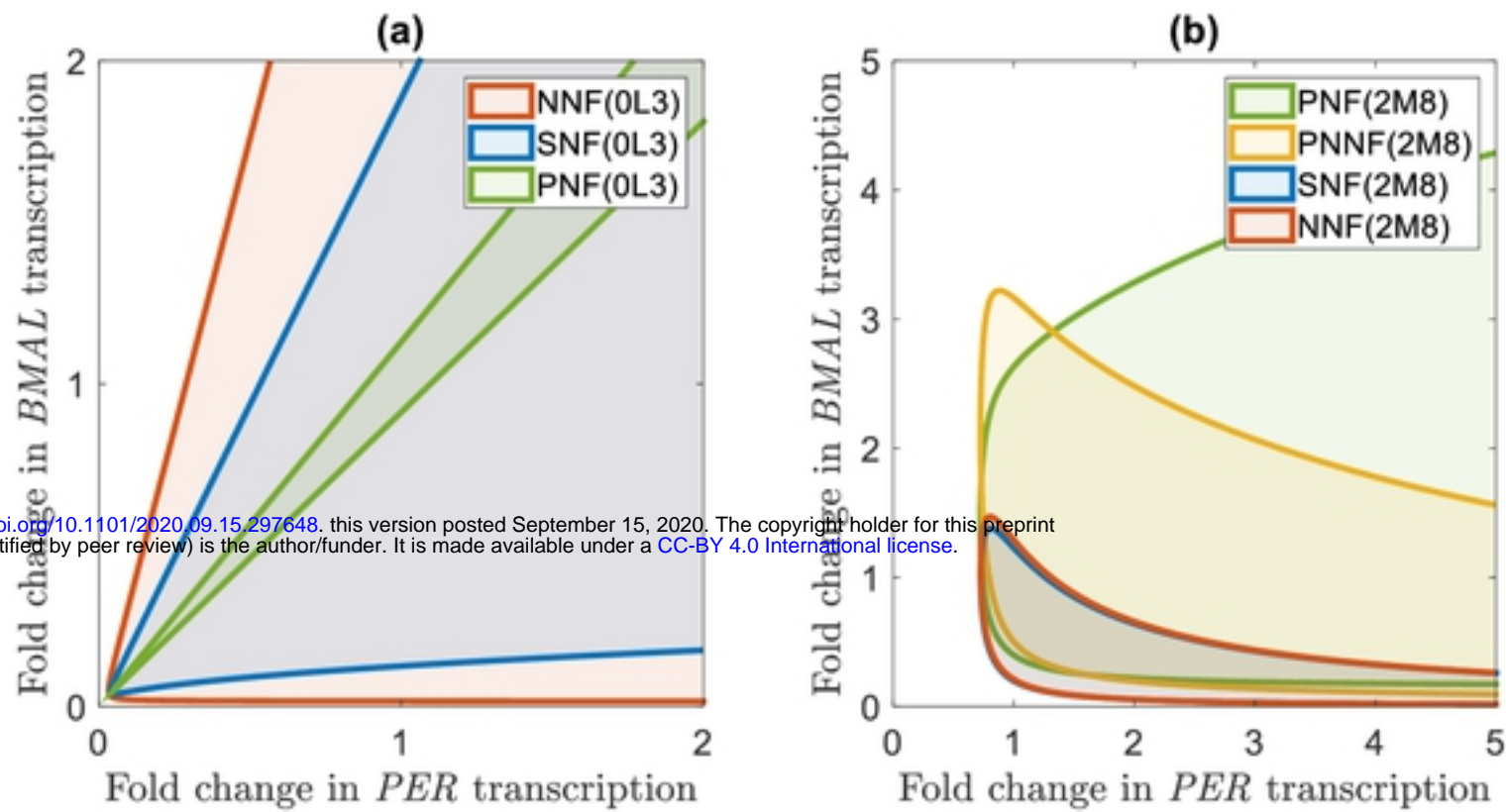
Figure 4. Two-parameter bifurcation curves with respect to fold changes in *BMAL* and *PER* transcription rates. **(a)** Comparison of oscillatory robustness for the unmodified KF models: SNF(0L3), NNF(0L3) and PNF(0L3). The *BMAL* transcription rate is varied with parameter A_T (for SNF) or γ (for NNF and PNF). $K_d = 10^{-5}$ in panel a (to allow oscillations in the unmodified KF models). **(b)** Comparison of oscillatory robustness for the modified KF models: SNF(2M8), NNF(2M8), PNF(2M8), PNNF(2M8). The *BMAL* transcription rate is varied with parameter A_T (for SNF) or A_{MAX} (for NNF, PNF and PNNF). $K_d = 10^{-1}$ in panel b. The *PER* transcription rate is varied with φ for all models. The other parameter values used in these calculations are provided in Table S4.

Figure 5. Two-parameter bifurcation curves with respect to fold changes in *BMAL* and *PER* transcription rates for **(a)** SNF(2M8), **(b)** NNF(2M8), **(c)** PNF(2M8), and **(d)** PNNF(2M8). Within the oscillatory regions, period is color-coded. The *BMAL* transcription rate is varied with parameters A_T (SNF) or A_{MAX} (NNF, PNF, PNNF). The *PER* transcription rate is varied with φ for all models. All parameter values for these calculations can be found in Table S4.